

Article

Environmentally Friendly Photoluminescent Coatings for Corrosion Sensing

Carmen R. Tubio ^{1,*}, Laura Garea ¹, Bárbara D. D. Cruz ^{2,3}, Daniela M. Correia ², Verónica de Zea Bermudez ⁴
and Senentxu Lanceros-Mendez ^{1,5}

- ¹ BCMaterials, Basque Center for Materials, Applications and Nanostructures, UPV/EHU Science Park, 48940 Leioa, Spain; laura.garea.mayordomo@gmail.com (L.G.); senentxu.lanceros@bcmaterials.net (S.L.-M.)
- ² Centre of Chemistry, University of Minho, 4710-057 Braga, Portugal; barbaraddcruz@gmail.com (B.D.D.C.); dcorreia@quimica.uminho.pt (D.M.C.)
- ³ Physics Centre of Minho and Porto Universities (CF-UM-UP) and Laboratory of Physics for Materials and Emergent Technologies (LapMET), University of Minho, 4710-057 Braga, Portugal
- ⁴ Chemistry Department and CQ-VR, University of Trás-os-Montes e Alto Douro, 5000-801 Vila Real, Portugal; vbermude@utad.pt
- ⁵ IKERBASQUE, Basque Foundation for Science, 48009 Bilbao, Spain
- * Correspondence: carmen.rial@bcmaterials.net

Abstract: Although an increasing number of studies are being devoted to the field of corrosion, with topics from protection to sensing strategies, there is still a lack of research based on environmentally eco-friendly materials, which is essential in the transition to sustainable technologies. Herein, environmentally friendly composites, based on photoluminescent salts dispersed in vegetable oil-based resins, are prepared and investigated as corrosion sensing coatings. Two salts NaA, where A⁻ is a lanthanide complex anion (with Ln = Nd³⁺, and Yb³⁺), are incorporated into the resins as active functional fillers and different coatings are prepared on carbon steel substrates to assess their functional properties. The influence exerted by a corrosive saline solution on the morphology, structural, and photoluminescent properties of the coatings is evaluated, and their suitability for the practical detection of the early corrosion of coated carbon steel is demonstrated. The photoluminescence of the composite coatings depends on the corrosion time, with the effect being more important for the coatings doped with Nd³⁺. The present work shows that the composites obtained are suitable candidates for corrosion sensing coating applications, offering improved sustainability.

Keywords: corrosion; photoluminescence salts; lanthanide complexes; sensing



Academic Editors: Tengling Ye and Bixin Li

Received: 17 December 2024

Revised: 27 January 2025

Accepted: 29 January 2025

Published: 31 January 2025

Citation: Tubio, C.R.; Garea, L.; Cruz, B.D.D.; Correia, D.M.; de Zea Bermudez, V.; Lanceros-Mendez, S. Environmentally Friendly Photoluminescent Coatings for Corrosion Sensing. *Polymers* **2025**, *17*, 389. <https://doi.org/10.3390/polym17030389>

Copyright: © 2025 by the authors. Licensee MDPI, Basel, Switzerland. This article is an open access article distributed under the terms and conditions of the Creative Commons Attribution (CC BY) license (<https://creativecommons.org/licenses/by/4.0/>).

1. Introduction

Undesired corrosion is a relevant problem in several sectors and industries, including the energy, transport, and automotive sectors. In addition, it is relevant to infrastructure, such as bridges, pipelines, and highways, among other areas [1]. Consequently, in the past decades, extensive research has been performed on the development of efficient strategies to improve the protection, continuous monitoring, and early detection of corrosion processes. The great majority of studies related to corrosion protection have focused on organic/inorganic coatings, the removal of corrosive constituents, the use of inhibitors, and anodic/cathodic protection [2–4]. In parallel, during the past decade, extensive self-repairing strategies have been introduced in protective coatings [5,6].

In addition to the well-established approaches, the implementation of sensing capabilities is recognized as one of the most effective ways to early detect, monitor, and

control corrosion processes. The implementation of sensing technologies essentially relies on the use of optical fibers [7,8], electrochemical noise detection [9,10], pH-indicating agents [11,12], and smart materials which can provide qualities of self-healing, damage sensing, and stimulus responsiveness [13,14]. In particular, fluorescence-based sensors have been proposed as a suitable sensing solution due to their high sensitivity and real-time detection [15]. Their working principle is based on the use of fluorescent indicators, which can be sensitive to pH or metal ion variations and can be added to solutions or coatings. Several reports have demonstrated that these fluorescent indicators can act as sensors, with promising results in the corrosion field [13,16]. However, one of the most critical issues is the design and synthesis of composites with environmentally friendly materials.

In this context, many luminescent salts are environmentally friendly compounds which properties can be tailored through the judicious choice of the nature of the cations and anions. This advantage, plus the fact those materials may be incorporated into specific polymer matrices, has boosted their use in a wide range of applications [17]. Concerning luminescence characteristics, the introduction of lanthanide metal ions, such as lanthanide (Ln^{3+}) ions, can yield highly luminescent compounds with narrow emission bands, photostability, long decay times, and high quantum efficiency [17,18]. The potential of luminescent salts has been exploited in various applications, such as anticounterfeiting [19,20] and biomedical imaging [21,22], among others [23–25]. Yet, in the field of corrosion sensing, such luminescent compounds have scarcely been explored. Therefore, taking into consideration the current pressing need for more sustainable approaches and materials, it is suitable to evaluate the use of luminescent materials as active fillers to develop practical sensors in the area of corrosion. Another important aspect is the selection of the host polymeric matrix, which should also be environmentally sustainable to reduce the use of synthetic materials and address the requirement of eco-friendly formulations towards sustainable materials, processes, and technologies. In this regard, vegetable oil-based resins have emerged as promising candidates on account of being abundantly available, and environmentally friendly. At present, vegetable resins are being increasingly employed in the coating industry, demonstrating potential applicability in corrosive environments [26].

In this work, we propose a novel approach to develop sensing materials for corrosive environments. This implies the use of a soybean-based vegetable UV-curable resin doped with $\text{Na}[\text{Ln}(\text{tta})_4]$, where $\text{Ln} = \text{Nd}$ or Yb and tta^- is tetrakis(thenoyltrifluoroacetate). The latter sodium salts are the precursor compounds of luminescent salts, the applicability of which has been already demonstrated in anticounterfeiting [19,20]. Herein, we demonstrate the applicability of such composite materials in corrosion sensing through the evaluation of the sensing performance in coated carbon steel substrates in saline environments. Accordingly, immersion experiments are performed in 5 wt. % NaCl solution for several days. In the present work, the coating is directly placed on top of the corroding surface, whereas in specific applications, such as very harsh environments, the sensing layer can be placed on top of another more protective layer. This work represents a basis for a new sensing approach in the area of steel corrosion, with improved performance and sustainability.

2. Materials and Methods

2.1. Materials

A transparent soybean-based and biodegradable photopolymer resin (ECO UV resin, Anyubic, Shenzhen, China) was used as received.

2-thenoyltrifluoroacetone (Htta) (99%, Sigma-Aldrich, St. Louis, MO, USA), ethanol (EtOH) (99.8%, Fisher Chemical, Loughborough, UK), neodymium(III)chloride hexahydrate $\text{NdCl}_3 \cdot 6\text{H}_2\text{O}$, 99.9%, Sigma-Aldrich, USA), ytterbium (III)chloride hexahydrate

($\text{YbCl}_3 \cdot 6\text{H}_2\text{O}$, 99.9%, Sigma-Aldrich), and sodium hydroxide (NaOH, Merck, Rahway, NJ, USA) were used as received.

2.2. Preparation of Ln-Based Salts

Two Ln ternary complexes were prepared according to the procedure reported in [19,20]. Briefly, the synthesis involved the dissolution of Htta in EtOH under magnetic stirring, followed by deprotonation with NaOH at 50–60 °C for 2 h. Then, $\text{NdCl}_3 \cdot 6\text{H}_2\text{O}$, was dissolved in EtOH and was added dropwise into the previous solution. The mixture was kept at 50–60 °C for 1 h, and then the EtOH was evaporated. Afterwards, the resultant salt was dried at 50 °C for 3 days. Similarly, $\text{Na}[\text{Yb}(\text{tta})_4]$ synthesis was achieved using $\text{YbCl}_3 \cdot 6\text{H}_2\text{O}$ as a lanthanide metal precursor. Figure 1 shows the chemical structure of $\text{Na}[\text{Ln}(\text{tta})_4]$, where Ln = Nd or Yb, and tta⁻ is tetrakis(thenyltrifluoroacetate).

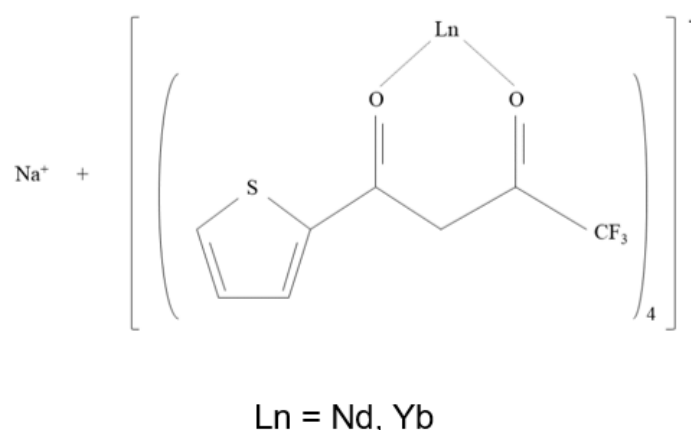


Figure 1. Chemical structure of $\text{Na}[\text{Ln}(\text{tta})_4]$.

2.3. Sample Preparation and Corrosion Experiments

The coating solutions were based on the vegetable UV-curable resin mixed with the sodium salts in a planetary mixer (Thinky ARE-250, Tokyo, Japan) at 2000 rpm for 4 min several times. The salt loading was controlled at 5 and 10 wt. %. Carbon steel substrates (DC01, Laser Norte S.A., Biscay, Spain) with dimensions of 5 mm × 2 mm × 0.5 mm were coated with the Ln-doped solutions using the doctor blade technique and the as-coated films were cured in a UV curing chamber (UVACUBE 400, Hönle AG, Gilching, Germany) for 3 min at 400 W.

The influence of saline solutions on the coated steel substrates was evaluated by immersing the samples in a 5 wt. % NaCl solution. This study was carried out for 4 days, and the results were evaluated on days 1 and 4. The nomenclature adopted to represent the prepared samples was resin-xLn (with x%wt.).

2.4. Characterization of the Samples

The Fourier Transform Infrared (FTIR) spectra were recorded on a Jasco FT/IR-6100 equipped with an Attenuated Total Reflection (ATR) accessory (Easton, MD, USA). The samples were scanned in the 600–4000 cm^{-1} spectral range with a 4 cm^{-1} resolution.

The morphology and elemental compositions of the samples were observed by a scanning electron microscope (SEM, Carl Zeiss EVO-40, Berlin, Germany) equipped with an energy-dispersive mode (EDX, Oxford Instruments, Abingdon, UK). Before the analysis, the samples were sputtered with a 10 nm thin gold layer.

Energy-dispersive X-ray fluorescence (ED-XRF) analysis was performed using the Spectro Midex SD system (Ametek, Inc., Leicester, UK).

Photoluminescence (PL) spectra were recorded using a fluorescence spectrometer (FLS980, Edinburgh Instruments Ltd., Livingston, UK) with a Xenon lamp 450 W. The excitation wavelength was 300 nm.

3. Results

3.1. Active Coating Characterization

FTIR analysis was carried out to evaluate the nature of the interactions between the UV-curable resin matrix and the Na[Ln(tta)₄] salts. The FTIR spectra of the neat resin and resin-10Ln (Ln = Nd and Yb) samples in the 3000–600 cm⁻¹ wavenumber range are shown in Figure 2.

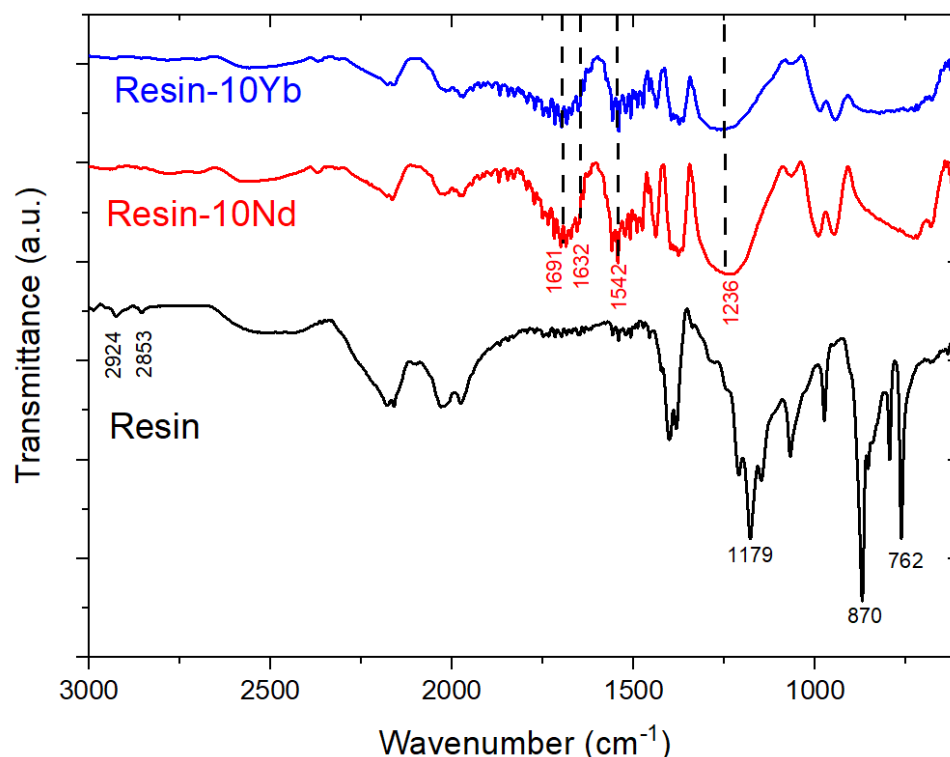


Figure 2. FTIR spectra of the neat resin and resin-10Ln samples.

The FTIR signature of the doped samples was markedly different from that of the neat resin. The FTIR spectrum of the pristine resin showed the typical bands of soybean oil [27–29]. In particular, the characteristic bands of the C–O bond were observed at 1179 cm⁻¹, as were the bands at 2924 and 2853 cm⁻¹. This was related to the presence of the weak asymmetric stretching of the –C–H bond. In addition, the bands of higher intensity at 870 and 762 cm⁻¹ allowed us to identify the =C–H bond bending mode. On the other hand, with the presence of the Ln-based salts, new peaks were identified in the composites. These were related to the presence of the filler. In particular, bands that were specific to the β -diketonate ligand were identified at 1542 cm⁻¹ due to the presence of the C=C bond, at 1691 and 1632 cm⁻¹, which was ascribed to the carbonyl (C=O) group, and at 1236 cm⁻¹, which was associated with the C–CF₃ group [30]. No new bands or energy shifts of the resin and Ln-based salts bands were observed in the composites, indicating a lack of strong interactions between the different composite components.

To study the morphology and microstructure of the samples, SEM and EDX measurements were performed (Figure 3). Figure 3a shows a representative SEM image taken from the cross-sectional area of the neat resin, and the corresponding EDX mapping of the C and O elements. The SEM image reveals that the as-prepared sample is characterized by

a smooth and compact morphology, where C and O are homogeneously distributed all along the polymer. The relative distribution of these elements was in agreement with the composition of the vegetable resin made from soybean oil. Furthermore, as observed in Figure 3b,c, the dense morphology was maintained after salt addition and the corresponding EDS map demonstrates the uniform distribution of C, O, Nd, and Yb within the resin matrix, i.e., the excellent distribution of the filler within the polymer matrix, with no large aggregates or voids.

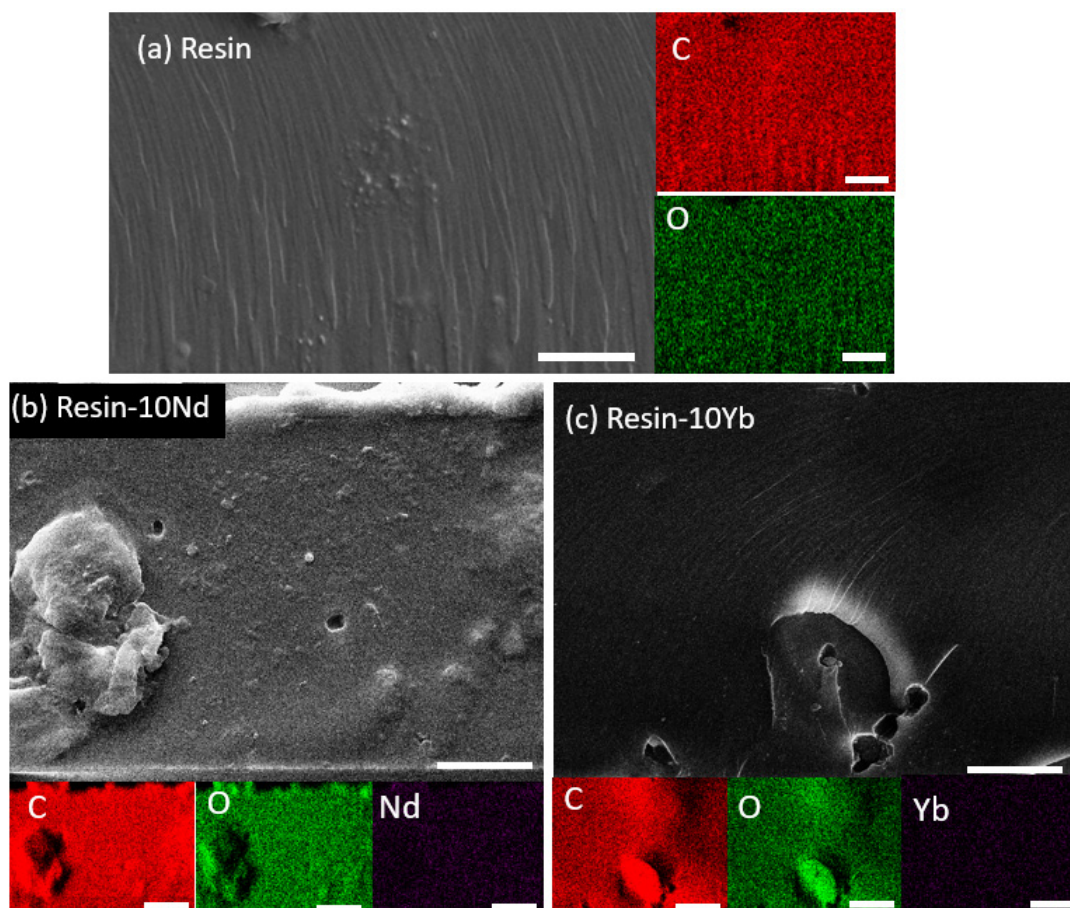


Figure 3. Cross-sectional SEM image and corresponding EDS elemental mapping of the resin-xLn as-prepared samples: (a) neat resin; (b) resin-10Nd; (c) resin-10Yb. Scale bar: 10 μm .

3.2. Corrosion Tests

Figure 4 shows the SEM images of the samples doped with 10 wt. % of $\text{Na}[\text{Ln}(\text{tta})_4]$ before and after immersion in 5 wt. % NaCl solution. A roughened morphology with defects was visible for the samples treated for 1 and 4 days, indicating that the saline solution caused significant corrosive attack on the samples. Additionally, the EDX results represented in Table 1 evidence the high content of C and O elements in all the samples. As expected, the samples contained elements of $\text{Na}[\text{Ln}(\text{tta})_4]$ before and after immersion in the saline solution. Importantly, we noticed that small quantities of Fe were found in the samples exposed to the saline solution for 4 days. This was associated with the corrosion process of the carbon steel substrate. The findings are presented in Figure 5, with the EDX mapping images showing the homogeneous distribution of Fe elements.

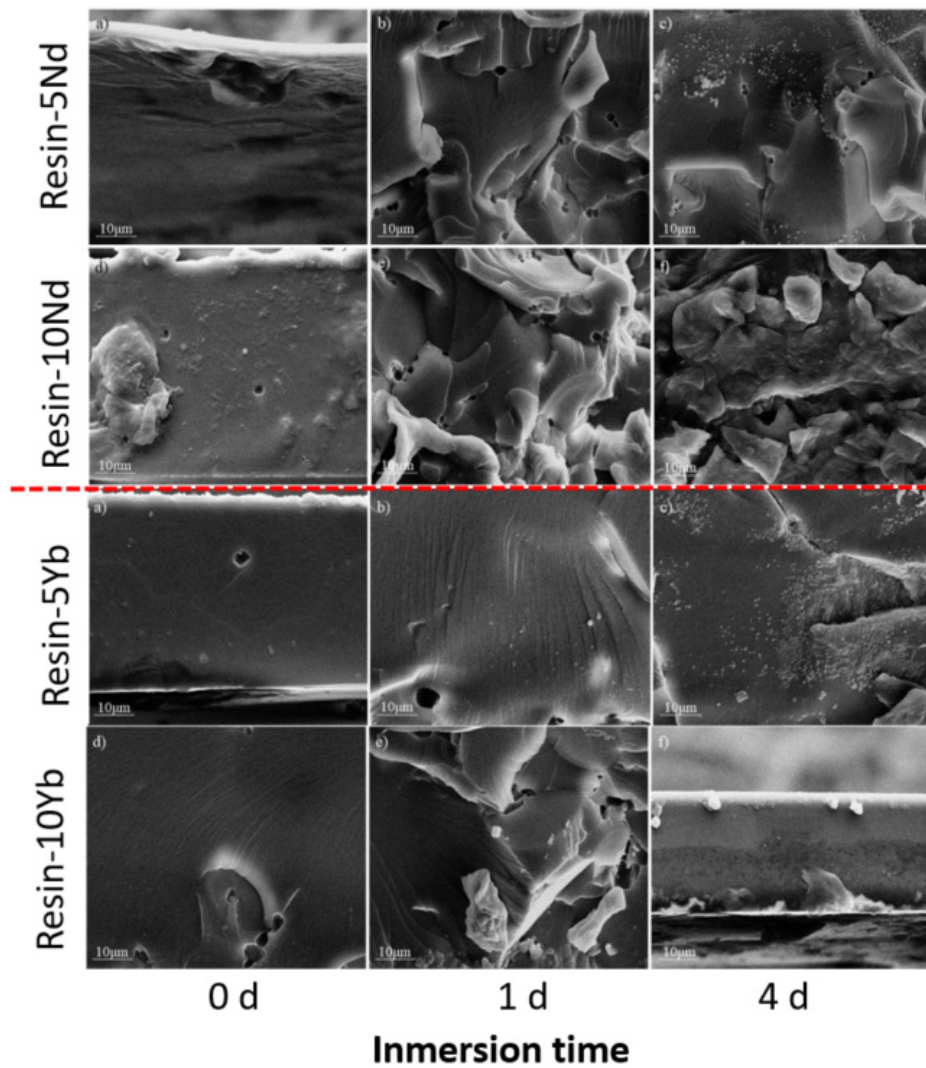


Figure 4. SEM images of the resin-xLn samples before and after immersion in 5 wt. % NaCl for 1 and 4 days. The scale is 10 μm .

Table 1. Elemental compositions of the resin-xLn as a function of immersion time (t_i) in the NaCl solution as calculated by EDX.

Ln	x	t_i (day)	Elemental Composition (wt. %)								
			C	O	Cl	Ln	F	Na	K	Ca	Fe
Nd	5	0	70.02	26.19	0.99	0.49	0.84	0.46	0.74	0.25	0
		1	67.27	29.49	0.45	0.69	1.76	0.34	0	0	0
		4	65.85	31.04	0.51	0.38	1.09	0.5	0	0	0.62
	10	0	63.36	30.24	1.07	1.02	3.03	0.73	0.37	0.19	0
		1	60.17	34.1	0.74	0.99	3.04	0.45	0.41	0.1	0
		4	64.95	29.82	0.37	1.12	2.8	0.32	0	0	0.62
Yb	5	0	62.48	34.25	0.17	0.53	1.82	0.19	0.07	0.08	0
		1	67.32	29.2	0.23	0.65	1.4	0	0	0	0
		4	60.15	28.19	4.13	0.57	0.88	4.53	0.08	0	0.96
	10	0	66.04	27.62	0.2	1.58	2.67	0.22	0	0	0
		1	57.45	34.54	1.49	1.43	2.87	0.98	0.59	0.65	0
		4	60.67	32.39	0.37	1.39	2.71	0.35	0.27	0.7	0.18

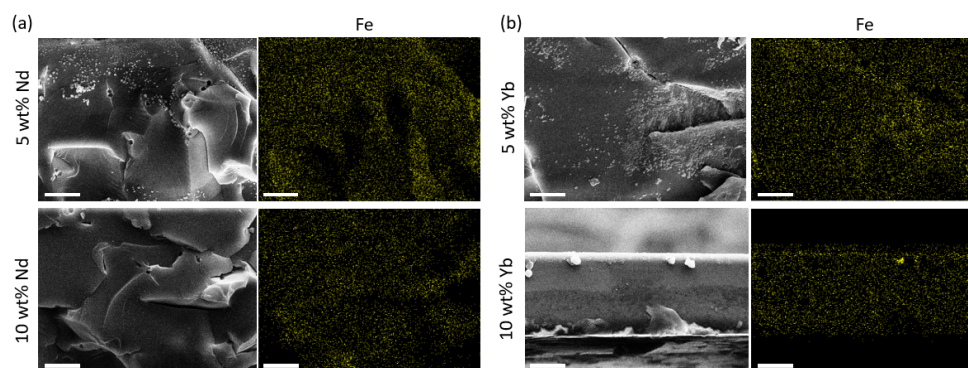


Figure 5. SEM images and corresponding EDS elemental mapping for the distribution of Fe elements in the resin-xLn after immersion in 5 wt. % NaCl for 4 days: (a) resin-5Nd (up) and resin-10Nd (down), and (b) resin-5Yb (up) and resin-10Yb (down). Scale bar: 10 μm .

The results obtained from the EDX analysis were complemented with an XRF test. Figure 6a and Table 1 depict the Fe contents found in the coatings after 1 and 4 days of immersion in the saline solution, showing that the Fe contents increased with the increasing immersion time, revealing the effect of the Cl^- ions on the carbon steel substrate. Thus, substrate corrosion leads to Fe diffusion within the coating, as illustrated in Figure 6b. In addition, it is important to draw attention to the differences found with respect to the above EDX analysis. Both XRF and EDX are analytical tools for semi-quantitative elemental analysis, and they have different detection limits. While EDX tends to be more effective for lighter elements, XRF shows the opposite trend.

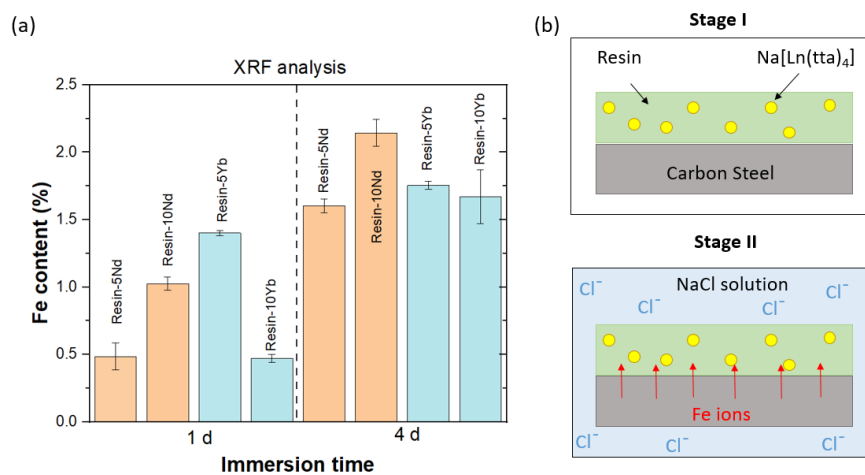


Figure 6. (a) A comparison of the Fe content values of the resin-xLn samples after 1 and 4 immersion days in 5 wt. % NaCl solution, as determined by XRF testing. (b) A schematic illustration of the system in the initial stage and after immersion in 5 wt. % NaCl solution.

Finally, the functional performance of the systems was evaluated. The PL spectra were measured to determine the sensing efficiency of the coatings against steel corrosion within the saline solution. Figure 7 show the PL changes of the resin with 10 wt. % of $\text{Na}[\text{Ln}(\text{tta})_4]$ for $\text{Ln} = \text{Nd}^{3+}$ and Yb^{3+} , respectively, as a function of exposure time to a saline medium. In the case of the sample doped with Nd^{3+} (Figure 7a), one emission band, peaking at 1058 nm, is observed. In contrast, in the case of the resin incorporating Yb^{3+} (Figure 7b), two distinct peaks are identified at 976 nm (sharp) and around 1000 nm (broad). These results are in agreement with the characteristic emission wavelengths of these lanthanide ions, with the 1058 and 976 nm peaks corresponding to the characteristic

Nd^{3+} (${}^4\text{F}_{3/2} \rightarrow {}^4\text{I}_{11/2}$) and Yb^{3+} (${}^2\text{F}_{5/2} \rightarrow {}^2\text{F}_{7/2}$) intra-4f transitions in the near-infrared (NIR) spectral range, respectively [31].

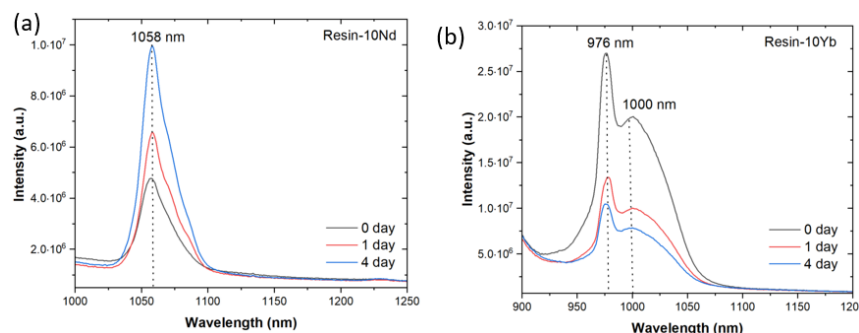


Figure 7. Emission spectra of the resin-10Ln samples, excited at 300 nm, before and after 1 and 4 immersion days in 5 wt. % NaCl solution: (a) Ln = Nd and (b) Ln = Yb.

With respect to the effect of the immersion time on the PL spectra, the first observation is that the intensity of the PL emission gradually increases in the case of the sample containing Nd^{3+} ions (Figure 7a), whereas a decrease in intensity is observed for the sample doped with Yb^{3+} (Figure 7b), showing the significant differences of both ions upon exposure to a corrosive medium. Those differences are related to the specific characteristics of the ions, including the luminescence lifetime, cross-sectional energy gap, and quantum efficiency, among others, as well as their different interactions with the host matrix. For example, Nd^{3+} has a large energy gap between the most dominantly emissive ${}^4\text{F}_{3/2}$ spin orbit level and the lower ${}^4\text{I}_{5/2}$ level, while Yb^{3+} possesses a large absorption cross section of around 980 nm. In fact, this effect is also reported in related studies, regarding emission variations in lanthanide compounds, for sensing applications [32–34]. The values of the variation in the PL intensity as a function of time have also been determined. The PL intensity of Nd^{3+} increases up to around 27% after 1 day and 52% after 4 days. Meanwhile, for the 976 nm emission transition of Yb^{3+} , this percentage difference is reduced in 50.3% after 1 day and 61.13% after 4 days. This result is in accordance with the observed reduction in the 1000 nm band, with variations of up to 50.13% and 60.95% found after 1 and 4 days, respectively.

The obtained PL emission intensity results suggest that resins containing a functional luminescent lanthanide complex salt can potentially interact with the Fe compound and change the PL properties. They absorb energy and transfer it to the lanthanide metal to enhance the luminescence intensity or quench the luminescent signal. Several works have attempted to develop luminescent Ln-based sensors for Fe detection. For example, Orcutt et al. [35] developed a lanthanide-based chemosensor for bioavailable Fe^{3+} . The studies showed that the displacement of the lanthanide-associated bands with Fe (III) is achieved in organic solvents. Yu et al. [36] demonstrated that several lanthanide metal–organic framework (MOF) compounds present an ultra-sensitive luminescent sensing response towards Fe (III). In addition, Fan et al. [37] studied the application of lanthanide compounds as fluorescent sensors for Fe (III). The results showed that samples are highly selective and sensitive luminescence probes for Fe (III) ions. Focusing on the luminescent sensing mechanism in these previous studies, it is related to variations in the charge transfer and energy transfer transitions. Despite these advances in designing sensors for iron detection, there are still challenges to overcome, such as improving the understanding the energy level modifications and electron–photon coupling parameters, which can provide deeper insights about luminescence sensing mechanisms. Therefore, it is necessary to support experimental analysis with theoretical methods, such as frontier molecular orbital analysis or quantum chemical approaches.

Thus, the variation in the PL emission spectra of the coatings in the presence of Fe ions allows us to monitor the evolution of corrosion over time. Therefore, they work as corrosion sensing coatings. Further, the sensing layer can be placed directly on the corroding surface or on top of another protective layer in a multilayer protective sensing system.

4. Conclusions

This study focused on the development of sustainable coatings with the ability of sensing corrosion. Specifically, the composite coatings fabricated by the combination of luminescent salts and the soybean vegetable matrix were applied to carbon steel substrates, and the system was stored in a saline medium. The morphological and structural features of samples were studied and the results were confirmed by the effective corrosion of carbon steel in the saline solution. Importantly, the functional sensing capability was evaluated through the variation in the PL of the coatings. The PL results show that the type of filler plays a profound role in the sensing response, the Nd-based salt showing a better performance than the Yb-based salt. Our results demonstrate that composites based on eco-friendly and sustainable materials show great potential to be used in sensing-based devices for corrosive environments.

Author Contributions: Conceptualization, C.R.T. and S.L.-M.; methodology, C.R.T. and S.L.-M.; validation, C.R.T.; formal analysis, C.R.T., L.G., B.D.D.C., D.M.C., V.d.Z.B. and S.L.-M.; investigation, C.R.T., L.G., B.D.D.C., D.M.C., V.d.Z.B. and S.L.-M.; resources, S.L.-M.; data curation, C.R.T., L.G., B.D.D.C., D.M.C. and V.d.Z.B.; writing—original draft preparation, C.R.T., D.M.C. and V.d.Z.B.; writing—review and editing, C.R.T. and S.L.-M.; supervision, C.R.T. and S.L.-M.; project administration, S.L.-M.; funding acquisition, S.L.-M. All authors have read and agreed to the published version of the manuscript.

Funding: This study forms part of the Advanced Materials programme and was supported by MCIN with funding from European Union NextGenerationEU (PRTR-C17.I1) as well as by IKUR Strategy under the collaboration agreement between Ikerbasque Foundation and Fundación BCMaterials on behalf of the Department of Education of the Basque Government. Funding from the Basque Government Industry Department under the ELKARTEK program is also acknowledged. The authors thank the Fundação para a Ciência e Tecnologia (FCT) for financial Support under the framework of Strategic Funding UID/QUI/00686/2020 and UID/FIS/04650/2020 and the Investigator FCT Contract 2020.02915.CEECIND (10.54499/2020.02915.CEECIND/CP1600/CT0029) (D.M.C.).

Institutional Review Board Statement: Not applicable.

Informed Consent Statement: Not applicable.

Data Availability Statement: Data are contained within the article.

Acknowledgments: Technical and human support provided by Sgiker (UPV/EHU) and University of Burgos (UBU) are gratefully acknowledged.

Conflicts of Interest: The authors declare no conflict of interest.

References

1. National Research Council; Committee on Research Opportunities in Corrosion Science and Engineering. *Research Opportunities in Corrosion Science and Engineering*; The National Academies Press: Washington, DC, USA, 2011.
2. Leal, D.A.; Kuznetsova, A.; Silva, G.M.; Tedim, J.; Wypych, F.; Marino, C.E.B. Layered materials as nanocontainers for active corrosion protection: A brief review. *Appl. Clay Sci.* **2022**, *225*, 106537. [[CrossRef](#)]
3. Alao, A.O.; Popoola, A.P.; Sanni, O. The Influence of Nanoparticle Inhibitors on the Corrosion Protection of Some Industrial Metals: A Review. *J. Bio-Tribo-Corros.* **2022**, *8*, 68. [[CrossRef](#)]
4. Refait, P.; Grolleau, A.-M.; Jeannin, M.; Sabot, R. Cathodic Protection of Complex Carbon Steel Structures in Seawater. *Corros. Mater. Degrad.* **2022**, *3*, 439–453. [[CrossRef](#)]

5. Poornima Vijayan, P.; Al-Maadeed, M. Self-Repairing Composites for Corrosion Protection: A Review on Recent Strategies and Evaluation Methods. *Materials* **2019**, *12*, 2754. [[CrossRef](#)]
6. Liu, C.; Wu, H.; Qiang, Y.; Zhao, H.; Wang, L. Design of smart protective coatings with autonomous self-healing and early corrosion reporting properties. *Corros. Sci.* **2021**, *184*, 109355. [[CrossRef](#)]
7. Dong, S.; Liao, Y.; Tian, Q.; Luo, Y.; Qiu, Z.; Song, S. Optical and electrochemical measurements for optical fibre corrosion sensing techniques. *Corros. Sci.* **2006**, *48*, 1746–1756. [[CrossRef](#)]
8. Sousa, I.; Pereira, L.; Mesquita, E.; Souza, V.L.; Araújo, W.S.; Cabral, A.; Alberto, N.; Varum, H.; Antunes, P. Sensing System Based on FBG for Corrosion Monitoring in Metallic Structures. *Sensors* **2022**, *22*, 5947. [[CrossRef](#)]
9. Tan, Y. Sensing localised corrosion by means of electrochemical noise detection and analysis. *Sens. Actuators B Chem.* **2009**, *139*, 688–698. [[CrossRef](#)]
10. Permeh, S.; Lau, K. Electrochemical Behavior of Steel in Alkaline Sulfate Solutions with Low Level Chloride Concentrations. *Meet. Abstr.* **2021**, MA2021-02, 598. [[CrossRef](#)]
11. Maia, F.; Tedim, J.; Bastos, A.C.; Ferreira, M.G.S.; Zheludkevich, M.L. Nanocontainer-based corrosion sensing coating. *Nanotechnology* **2013**, *24*, 415502. [[CrossRef](#)]
12. Dararatana, N.; Seidi, F.; Crespy, D. PH-Sensitive Polymer Conjugates for Anticorrosion and Corrosion Sensing. *ACS Appl. Mater. Interfaces* **2018**, *10*, 20876–20883. [[CrossRef](#)] [[PubMed](#)]
13. Augustyniak, A.; Tsavalas, J.; Ming, W. Early detection of steel corrosion via “turn-on” fluorescence in smart epoxy coatings. *ACS Appl. Mater. Interfaces* **2009**, *1*, 2618–2623. [[CrossRef](#)] [[PubMed](#)]
14. Liu, C.; Qian, B.; Hou, P.; Song, Z. Stimulus Responsive Zeolitic Imidazolate Framework to Achieve Corrosion Sensing and Active Protecting in Polymeric Coatings. *ACS Appl. Mater. Interfaces* **2021**, *13*, 4429–4441. [[CrossRef](#)]
15. Chen, C.; Yu, M.; Tong, J.; Xiong, L.; Li, Y.; Kong, X.; Liu, J.; Li, S. A review of fluorescence based corrosion detection of metals. *Corros. Commun.* **2022**, *6*, 1–15. [[CrossRef](#)]
16. Su, F.; Du, X.; Shen, T.; Qin, A.; Li, W. Aggregation-induced emission luminogens sensors: Sensitive fluorescence ‘Turn-On’ response for pH and visually chemosensing on early detection of metal corrosion. *Prog. Org. Coat.* **2021**, *153*, 106122. [[CrossRef](#)]
17. Zhang, S.; Zhang, Q.; Zhang, Y.; Chen, Z.; Watanabe, M.; Deng, Y. Beyond solvents and electrolytes: Ionic liquids-based advanced functional materials. *Prog. Mater. Sci.* **2016**, *77*, 80–124. [[CrossRef](#)]
18. Tang, S.F.; Mudring, A.V. Highly Luminescent Ionic Liquids Based on Complex Lanthanide Saccharinates. *Inorg. Chem.* **2019**, *58*, 11569–11578. [[CrossRef](#)]
19. Correia, D.M.; Polícia, R.; Pereira, N.; Tubio, C.R.; Cardoso, M.; Botelho, G.; Ferreira, R.A.S.; Lanceros-Méndez, S.; de Zea Bermudez, V. Luminescent Poly(vinylidene fluoride)-Based Inks for Anticounterfeiting Applications. *Adv. Photonics Res.* **2022**, *3*, 2100151. [[CrossRef](#)]
20. Cruz, B.D.D.; Correia, D.M.; Polícia, R.; Pereira, N.; Nunes, P.; Fernandes, M.; Tubio, C.R.; Botelho, G.; Lanceros-Méndez, S.; de Zea-Bermudez, V. Photoluminescent alginate-based composite inks for anti-counterfeiting security and soft actuator applications. *Chem. Eng. J.* **2023**, *472*, 144813. [[CrossRef](#)]
21. Wang, W.; Fu, A.; Lan, J.; Gao, G.; You, J.; Chen, L. Rational Design of Fluorescent Bioimaging Probes by Controlling the Aggregation Behavior of Squaraines: A Special Effect of Ionic Liquid Pendants. *Chem. Eur. J.* **2010**, *16*, 5129–5137. [[CrossRef](#)]
22. Bwambok, D.K.; El-Zahab, B.; Challa, S.K.; Li, M.; Chandler, L.; Baker, G.A.; Warner, I.M. Near-Infrared Fluorescent NanoGUM-BOS for Biomedical Imaging. *ACS Nano* **2009**, *3*, 3854–3860. [[CrossRef](#)] [[PubMed](#)]
23. Chen, X.-W.; Liu, J.-W.; Wang, J.-H. A highly fluorescent hydrophilic ionic liquid as a potential probe for the sensing of biomacromolecules. *J. Phys. Chem. B* **2011**, *115*, 1524–1530. [[CrossRef](#)] [[PubMed](#)]
24. Bwambok, D.K.; Challa, S.K.; Lowry, M.; Warner, I.M. Amino acid-based fluorescent chiral ionic liquid for enantiomeric recognition. *Anal. Chem.* **2010**, *82*, 5028–5037. [[CrossRef](#)] [[PubMed](#)]
25. Loe-Mie, F.; Marchand, G.; Berthier, J.; Sarrut, N.; Pucheault, M.; Blanchard-Desce, M.; Vinet, F.; Vaultier, M. Towards an efficient microsystem for the real-time detection and quantification of mercury in water based on a specifically designed fluorogenic binary task-specific ionic liquid. *Angew. Chem. Int. Ed.* **2010**, *49*, 424–427. [[CrossRef](#)]
26. Sharmin, E.; Zafar, F.; Akram, D.; Alam, M.; Ahmad, S. Recent advances in vegetable oils based environment friendly coatings: A review. *Ind. Crops Prod.* **2015**, *76*, 215–229. [[CrossRef](#)]
27. Saremi, K.; Tabarsa, T.; Shakeri, A.; Babanalbandi, A. Epoxidation of Soybean Oil. *Ann. Biol. Res.* **2012**, *3*, 4254–4258.
28. Wang, R.; Schuman, T.P. Vegetable Oil-derived Epoxy Monomers and Polymer Blends: A Comparative Study with Review. *Express Polym. Lett.* **2013**, *7*, 272–292. [[CrossRef](#)]
29. Zhao, K.; Shi, L.; Liu, Z.; Li, J. Quality Analysis of Reheated Oils by Fourier Transform Infrared Spectroscopy. In Proceedings of the 2015 International Conference on Electromechanical Control Technology and Transportation, Zhuhai, China, 31 October–1 November 2015; pp. 245–249. [[CrossRef](#)]
30. Medina-Velazquez, D.Y.; Barraza, M.; Barron, M.; Hileio, I.; Colin, V. Influence of Synthesis Parameters on Luminescence of Thenoyltrifluoroacetone Europium Powders. *J. Mater. Sci. Chem. Eng.* **2018**, *6*, 1–8. [[CrossRef](#)]

31. Wang, R.; Zhang, F. CHAPTER 1 Lanthanide-Based Near Infrared Nanomaterials for Bioimaging. In *Near Infrared Nanomaterials: Preparation, Bioimaging, and Therapy Applications*; Nanoscience and Nanotechnology Series; Royal Society of Chemistry: London, UK, 2016; pp. 1–39. [[CrossRef](#)]
32. Suta, M.; Antić, Ž.; Đorđević, V.; Kuzman, S.; Dramićanin, M.D.; Meijerink, A. Making Nd³⁺ a Sensitive Luminescent Thermometer for Physiological Temperatures—An Account of Pitfalls in Boltzmann Thermometry. *Nanomaterials* **2020**, *10*, 543. [[CrossRef](#)]
33. Pedraza, F.J.; Rightsell, C.; Kumar, G.A.; Giuliani, J.; Monton, C.; Sardar, D.K. Emission Enhancement through Nd³⁺-Yb³⁺ Energy Transfer in Multifunctional NaGdF₄ Nanocrystals. *Appl. Phys. Lett.* **2017**, *110*, 223107. [[CrossRef](#)]
34. Aulsebrook, M.L.; Graham, B.; Grace, M.R.; Tuck, K.L. Lanthanide complexes for luminescence-based sensing of low molecular weight analytes. *Coord. Chem. Rev.* **2018**, *375*, 191–220. [[CrossRef](#)]
35. Orcutt, K.M.; Jones, W.S.; McDonald, A.; Schrock, D.; Wallace, K.J. A Lanthanide-Based Chemosensor for Bioavailable Fe³⁺ Using a Fluorescent Siderophore: An Assay Displacement Approach. *Sensors* **2010**, *10*, 1326–1337. [[CrossRef](#)] [[PubMed](#)]
36. Yu, X.; Ryadun, A.A.; Pavlov, D.I.; Guiselnikova, T.Y.; Potapov, A.S.; Fedin, V.P. Highly Luminescent Lanthanide Metal-Organic Frameworks with Tunable Color for Nanomolar Detection of Iron(III), Ofloxacin and Gossypol and Anti-counterfeiting Applications. *Angew. Chem. Int. Ed.* **2023**, *62*, e202306680. [[CrossRef](#)] [[PubMed](#)]
37. Fan, B.; Wei, J.; Ma, X.; Bu, X.; Xing, N.; Pan, Y.; Zheng, L.; Guan, W. Synthesis of Lanthanide-Based Room Temperature Ionic Liquids with Strong Luminescence and Selective Sensing of Fe(III) over Mixed Metal Ions. *Ind. Eng. Chem. Res.* **2016**, *55*, 2267–2271. [[CrossRef](#)]

Disclaimer/Publisher’s Note: The statements, opinions and data contained in all publications are solely those of the individual author(s) and contributor(s) and not of MDPI and/or the editor(s). MDPI and/or the editor(s) disclaim responsibility for any injury to people or property resulting from any ideas, methods, instructions or products referred to in the content.